JEEAR, Vol. 3 (1), 2024

DOI: 10.34002/jeear.v3i1.82

RESEARCH ARTICLE

X-ray Diffraction Analysis of Natural Calcite Minerals Found in General Santos City and Sarangani Province, Southern Philippines by Williamson–Hall Method

Raymond Benedict C. Dardo[1], Rommel J. Jagus[2], Masataka Imura[3], and Ryan G. Banal[4*]

[1] Mechanical Engineering Department, College of Engineering,
Mindanao State University − General Santos, Fatima, General Santos City, 9500 Philippines
[2] Information Technology and Physics Department, College of Natural Sciences and Mathematics,
Mindanao State University − General Santos, Fatima, General Santos City, 9500 Philippines
[3] Wide Bandgap Materials Group, National Institute for Materials Science,
1-1 Namiki, Tsukuba City, 305-0044, Japan
[4] Electrical and Electronics Engineering Department, College of Engineering,
Mindanao State University − General Santos, Fatima, General Santos City, 9500 Philippines
*Corresponding author: ryan.banal@msugensan.edu.ph

Received: November 20, 2023; Accepted: April 5, 2024; Published Online: April 12, 2024

Abstract

This study employs the Williamson–Hall (W–H) models to examine the microstrains and crystallite sizes of $CaCO_3$ occurring as calcite in limestone samples found in General Santos City and Sarangani Province, Southern Philippines. Using both the Uniform Deformation Model (UDM) and Uniform Stress Deformation (USDM) models, computations for average sizes were established to be identical, implying minimal strain influence. The consistency of resulting measurements extends to the microstrain, revealing uniform results for all samples. Correlation between crystallite sizes and microstrains in the calcite crystals was observed, where high-purity calcites exhibited larger crystallite sizes and microstrains. The crystallite sizes decrease with microstrains for calcites with higher Mg concentration, a finding that can be attributed to lattice distortion and the formation of defects. The release of stress forms these defects, thereby resulting in a reduction of microstrains. Moreover, the distinctly variable responses to strain exhibited by the samples could be influenced by either their anisotropic properties or other additional components. The W–H models, used jointly with UDM and USDM consistently predicted crystallite sizes, and thus offer valuable insights into the uniform stress responses of calcites. These promising results notwithstanding, USDM is shown to be especially relevant for anisotropic samples owing to the display deviations of crystallite sizes, a key feature of anisotropic natural calcites. The microscopic analysis is expected to provide additional understanding regarding the state of the limestone samples.

Keywords: *calcite, X-ray diffraction, Williamson–Hall analysis, crystallite size, microstrain*

Limestones are sedimentary rocks made of calcium carbonates ($CaCO_3$) [1-2] that exist as minerals in the form of calcites, aragonites, or valerite polymorphs phases [3-4]. These sedimentary rocks may contain a considerable amount of magnesium carbonate ($MgCO_3$), and calcium (Ca). One of these minerals is called dolomite, $MgCa(CO_3)_2$ [5]. Calcium carbonate is one of the most abundant minerals found on the Earth's crust [6]. It is most prevalent in warm, tropical, and subtropical seas where organisms such as algae, corals, snails, clams, and other organic debris that produce carbonate sediments thrive [6].

Limestones are used in many industrial and non-industrial applications [1, 5, 7], signifying their high economic value. Being the chief materials found in cement, aggregates, building stones, chalks, and crushed stones, limestones have found a wide array of applications in road/building constructions. They are also fired in kilns to produce cement, serve as dimension stones, and act as roofing granules providing weather- and heat-resistant coatings for roofing materials. Owing to their very high pH, limestones function as an agricultural lime (aglime) for the treatment of acidic soils. They are also important sources of

lime (CaO), and are used as pH regulators in the extraction of mineral gold from quartz, during laboratory-based dehydration and precipitation reactions in cement, glass, and paper industries, and in iron and steel-making [8-13].

Recently, the researchers confirmed that the limestone found in General Santos City and in other areas in Sarangani Province are mainly composed of the mineral calcites, which can consist of a combination with an aragonite phase [14]. Using X-ray diffraction (XRD) analysis, the variations in the *a* and *c* lattice constants of the calcite phase of the samples were due to the incorporation of magnesium (Mg) in the $CaCO_3$ lattice, resulting in alterations in their properties, the most apparent of which are the microstrains and crystallite sizes.

The substitution of Mg atoms into the lattice distorts a calcite crystal because of the smaller radius of Mg compared to Ca atoms. From having large (few micrometres) and ideally ordered crystalline array, the incorporation of Mg atoms may result into smaller crystallite sizes and microstrains. There are two types of lattice strain associated with nanocrystalline materials [15-16]. The first type extends over the entire lattice and is denoted by the shifts in the XRD peak positions. The second type extends only over a few lattice spacings and is often referred to as "microstrain" or "localized lattice strain" [17]. The microstrain is produced by residual stresses, vacancies, grain boundaries, faults, dislocations, and other defects that cause a non-uniform lattice distortion in the crystal. Hence, the microstrain is an indirect measure of the concentration of defects in the sample and can be a useful structural parameter for structure-property correlation [17].

The deviations from the perfect crystal lattice ordering extend in all directions, leading to the broadening of the diffraction peaks [18, 19]. The crystallite size and the microstrain are the two main properties that can be extracted from the peak width analysis of X-ray diffraction patterns. In the formation of polycrystalline aggregates, the crystallite size of the particle is not the same as the particle size, the crystallite size is considered as the smallest undistorted region in the crystal. The deviations due to the above contributions affect the Bragg peak by broadening (peak broadening) and correspondingly shifting its position.

In this paper, the XRD patterns of the natural calcite mineral found in some areas in Southern Philippines are analysed using the UDM and USDM models of the W–H method. In addition, the data gathered is used to look into the effect of the Mg incorporation on the quality of the calcite crystals obtained. The two analytical methods separate the crystallite size and microstrain contributions to the XRD line broadening. While the first method assumes a uniform deformation model (UDM) for elastically isotropic crystals, the other considers the anisotropic nature of the elastic constants of the crystal, using a uniform stress deformation model (USDM) [20-21]. The USDM model takes into account the anisotropic nature of the crystal and more often correctly predicts the system's property than those that do not take anisotropy into account, such as the UDM [17, 22-24]. The difference in results from both models would verify and quantify the anisotropy of the samples.

Materials and Methods

The sedimentary limestone samples were collected either from the boulders that are accumulated by the hill road during or the cut slope after road widening operations from different and random locations in General Santos City and Sarangani Province, taking into consideration their distances and ease of collection [14]. The samples were pulverized by mortar and pestle and classified using the Tyler sieve analysis. The pulverized samples were passed through a 200-mesh sieve, corresponding to a particle size of ~75 μm. To remove moisture, the samples were dried in an oven under an ambient atmosphere and at 105 °C for 12 hours. After cooling, the samples were stored either in a desiccator or in a sealed plastic bag to prevent moisture contamination.

The XRD analysis was carried out using the Rigaku MiniFlex 600 (Japan) to identify the type of minerals present in the samples and determine their crystallite sizes and microstrain. The X-ray radiation used was the Cu-Kα with a wavelength of 1.5406 Å, operated under 40 kV acceleration voltage and 10 mA current. The samples were scanned over a range of 10° to 90° at a scan rate of 20°/min.

Results and Discussion

XRD Analysis

The powder XRD patterns of the four different samples are shown in Figure 1. The sharp and narrow Bragg peaks indicate a high quality, good crystallinity, and fine grain size nature of the samples. The analysis of the XRD peaks confirmed the existence of calcite ($CaCO_3$) for all the samples, because the calcite has a trigonal crystal structure belonging to the hexagonal crystal system (JCPDS 05-0586) [25]. An aragonite phase was also confirmed in *Sample 2*. From the powder XRD data, the lattice constants were calculated to be a = 4.9794 - 4.9867 Å, and c = 17.0160 - 17.0555 Å, where the variation can be attributed to the Mg at different concentrations in the samples [14, 26-28]. The detailed identification process and

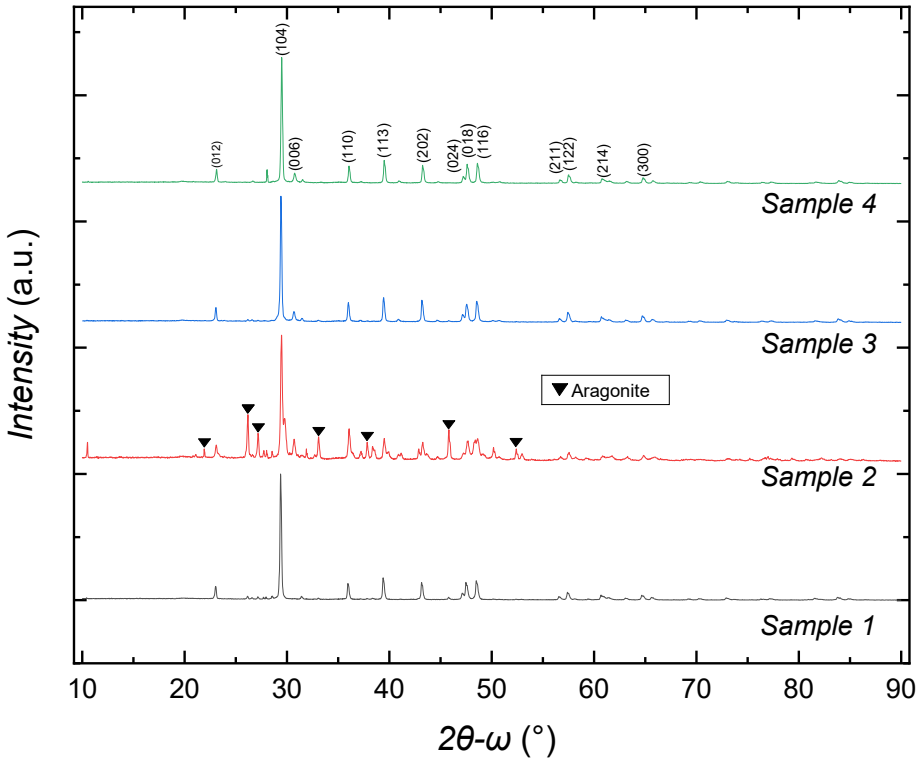

Figure 1. Powder X-ray diffraction profile of sedimentary limestone revealing high-quality calcite ($CaCO_3$) in all four samples (Pure calcite: JCPDS 05-0586).

analysis of the samples will be presented elsewhere [14].

Crystallite Size and Strain Analysis by Williamson–Hall Methods

Uniform Deformation Model (UDM)

Using the powdered XRD patterns, the crystallite size and microstrain were estimated from the broadening of the XRD linewidths. The linewidth broadening is mainly due to the instrumental effect, the crystallite size, and the lattice strain. The instrumental effect was eliminated using the following relation:

$$\beta_{hkl} = [(\beta_{hkl\ measured})^2 - (\beta_{hkl\ Instrumental})^2]^{1/2}. \quad (1)$$

The average crystallite size d was then alculated using the Debye–Scherrer formula [29-31]:

$$d = K\lambda / \beta_{hkl} \cos\theta_{hkl}, \quad (2)$$

where λ is the wavelength of the X-ray used (1.54056 Å), β_{hkl} the FWHM width of the diffraction peak, θ the diffraction angle, and K the Scherrer constant, commonly taken as 0.94.

Further, the strain ε induced in powders due to crystal imperfection and distortion was calculated using the formula:

$$\varepsilon = \beta_{hkl} / 4 \tan\theta_{hkl}. \quad (3)$$

Assuming that particle size and strain contribution to line broadening are independent of each other, then the observed line breadth is the sum of the crystallite size and strain:

$$\beta_{hkl} = K\lambda / d \cos\theta_{hkl} + 4\varepsilon \tan\theta_{hkl}. \quad (4)$$

By rearranging the equation, the Williamson–Hall equation [18] is written below.

$$\beta_{hkl} \cos\theta_{hkl} = K\lambda / d + 4\varepsilon \sin\theta_{hkl}, \quad (5)$$

Equation (5) represents the UDM, where the strain is assumed to be uniform in all crystallographic directions, giving the material properties independent of the direction along which they are measured.

Figure 2 (A, B, C, and D) plots the $4 \sin\theta$ along the x-axis and $\beta_{hkl} \cos\theta$ along the y-axis for all the samples using the UDM in the Williamson–Hall method. Meanwhile, Figure 2 (E, F, G, and H) demonstrate the plot of $4 \sin\theta / Y_{hkl}$ along the x-axis vs $\beta_{hkl} \cos\theta$ along the y-axis for all the samples using the USDM in the modified Williamson–Hall method. A linear fit is obtained for each particular case. From the linear fit data, the slope can be interpreted as strain ε and crystallite size d as the intercept.

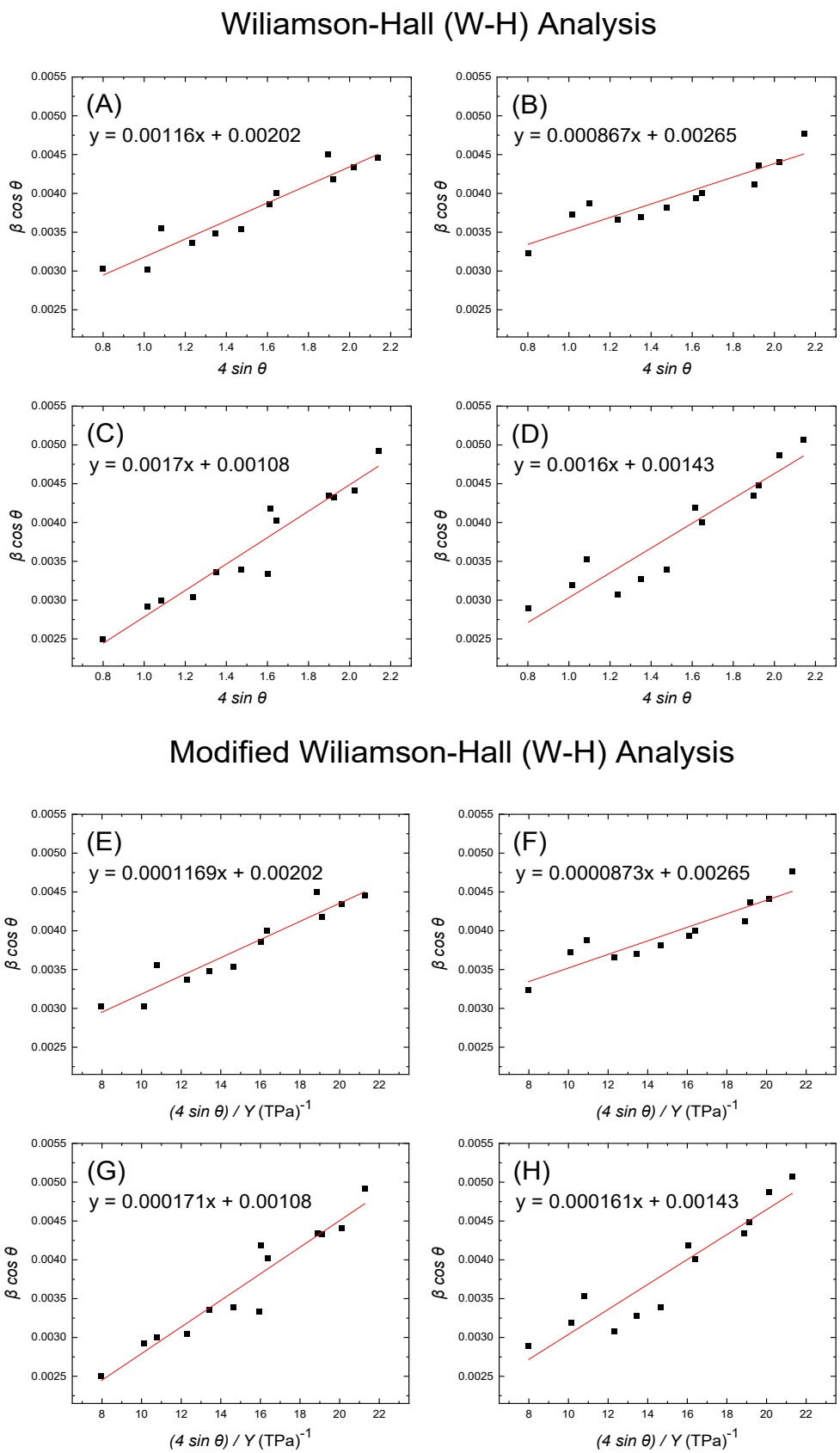

Figure 2. Microstrain and crystallite size measurement of calcite polymorphs in limestone samples using Williamson–Hall (W–H) and a modified W–H analysis. Microstrain and crystallite size for each sample: (A) and (E) for *Sample* 1, (B) and (F) for *Sample* 2 (C) and (G) for *Sample* 3, (D) and (H) *Sample* 4, was extracted using linear fitting.

Uniform Stress Deformation Model (USDM)

On the other hand, as crystals are generally anisotropic, the elastic constant is bound to be direction-dependent. Hence, the assumption in UDM that the strain has the same value in all crystallographic directions cannot be taken into an account in these samples. Therefore, the Williamson–Hall method is modified such that the anisotropic nature of the elastic constant is incorporated, hence now called USDM [20-21]. The deviations between the two models provide data that would quantify the anisotropic quality of the samples. In using USDM, within the elastic limit of the Hooke's law, there exists a linear proportionality relation between the stress σ and strain ε, given by $\sigma = \varepsilon Y_{hkl}$, where Y_{hkl} is the Young's modulus [32-33]. The W–H is thus modified accordingly by substituting the value of ε in Eq. (5):

$$\beta_{hkl} \cos\theta_{hkl} = K\lambda / d + 4\sigma \sin\theta / Y_{hkl}. \quad (6)$$

The Y_{hkl} is the crystallographic direction dependent in the direction perpendicular to the set of (hkl) planes. For hexagonal crystal, the Young's modulus equation and equations relating elastic compliances (S_{ij}) and stiffness constants (C_{ij}) are given by the following relation [31-36]:

$$Y_{hkl} = \frac{[h^2+\frac{(h+2k)^2}{3}+(\frac{al}{c})^2]^2}{S_{11}(h^2+\frac{(h+2k)^2}{3})^2+S_{33}(\frac{al}{c})^4+(2S_{13}+S_{44})(h^2+\frac{(h+2k)^2}{3})(\frac{al}{c})^2} \quad (7)$$

where

$S_{11} = C_{33}/2c + ½(C_{11}-C_{12})$,
$S_{13} = -C_{13}/c$, $S_{33} = (C_{11}+C_{12})/c$,
$S_{44} = 1/C_{44}$, $c = (C_{11}+C_{12})C_{33}-2C_{13}^2$.

The values of the four independent S_{ij}'s (in TPa^{-1}) are calculated by substituting correspondingly the C_{ij} (in GPa) constants [37], and thus obtaining the following values:

$S_{11} = 10.35$,
$S_{13} = -6.624$,
$S_{33} = 21.61$,
and $S_{44} = 28.57$.

Young's modulus calculated for all samples was ~100.5 GPa.

Table 1 summarizes the crystallite sizes and microstrains for all samples. Comparing the two models, the computed average crystallite sizes for all samples are nearly identical, indicating that introducing a strain in the W–H method has a minimal impact on the crystallite size of $CaCO_3$ particles. This is also the case for microstrain using both models for all samples. Moreover, a correlation exists between crystallite size and microstrain in the calcite crystal as larger crystallite sizes correspond to higher internal stress, and vice versa. *Sample 3* with the largest crystallite size indicates almost no Mg impurity in the $CaCO_3$ crystal. As Mg incorporation increases, the crystallite size decreases, denoting that substituting Ca with Mg could have reduced the crystallite size. This observation is evident in *Sample 2*, resulting in smaller crystallite size.

Figure 3 illustrates the relationship between the microstrains and the crystallite sizes of the samples. *Sample 3* exhibits the highest strain and largest crystallite size demonstrating that reducing the crystallite size increases strain. This lattice relaxation could be attributed to Mg substitution, as also observed in *Sample 4*. However, *Sample 1*, despite having a lesser amount of Mg substitution, displays a lesser strain compared to *Sample 4*. This is possibly influenced by the defects and dislocations already within the sample. In the case of *Sample 2*, which contains aragonite phases, there is less strain. The presence of aragonite could have also contributed to lattice relaxation although more studies are needed to elucidate this observation. Hence, the variation of

Table 1. Crystallite sizes and microstrains as calculated using USM and USDM.

	lattice constant		Williamson–Hall Analysis			
			USM		USDM	
Sample No.	a (Å)	c (Å)	d (nm)	ε (%)	d (nm)	ε (%)
Sample 1	4.9843	17.0555	71.7	0.0012	71.7	0.0012
Sample 2	4.9812	17.0173	54.6	0.00087	55.7	0.00087
Sample 3	4.9867	17.0476	134.1	0.0017	131.6	0.0017
Sample 4	4.9794	17.0558	101.3	0.0016	103.4	0.0016

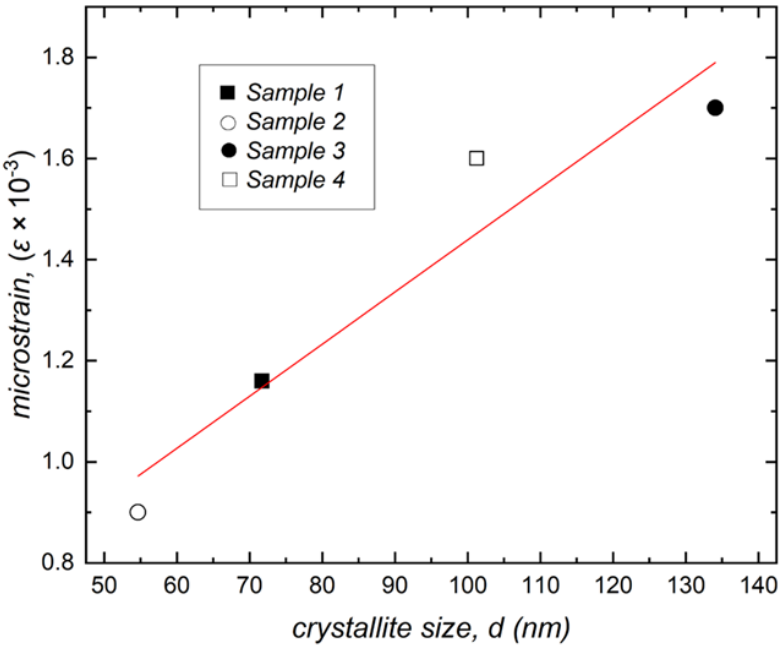

Figure 3. Microstrains and crystallite sizes correlation in the samples indicating *Sample* 3 of highest strain with the largest crystallite size, whereas *Sample* 4 demonstrates that decreasing crystallite size increases strain, potentially attributed to Mg substitution. *Sample* 1 show lesser strain despite lower Mg substitution, likely due to existing defects, while *Sample* 2 suggests lattice relaxation effects possibly due to the presence of the aragonite phase.

strain value could be directly influenced by the anisotropic nature and the presence of additional impurities within the samples.

Figure 4 shows the relationship between crystallite size (Fig. 4A) and microstrain (Fig. 4B) with the $CaCO_3$ lattice constants as obtained from the samples. Also shown in the figures is the plot of Mg incorporation with *a*- and *c*-lattice constants obtained from the JCPDS standard patterns (Pure calcite: JCPDS 05-0586, $Mg_{0.03}Ca_{0.9}7CO_3$: JCPDS 97-008-6161, and $Mg_{0.06}Ca_{0.94}CO_3$: JCPDS 89-1305). As observed, the *a*- and *c*-lattice constants decrease with increasing Mg concentration as expected. Hence, the lattice constants calculated from the XRD patterns of the samples can be attributed to their different Mg concentrations. Moreover, it can be observed that both microstrain and crystallite size are largest for the (almost) pure calcite sample, and decrease with increasing Mg concentration. Although the decreasing trend may not correlate exactly with that of either the crystallite size or microstrain, one can deduce that both the crystallite size and the microstrain decrease with the incorporation of Mg

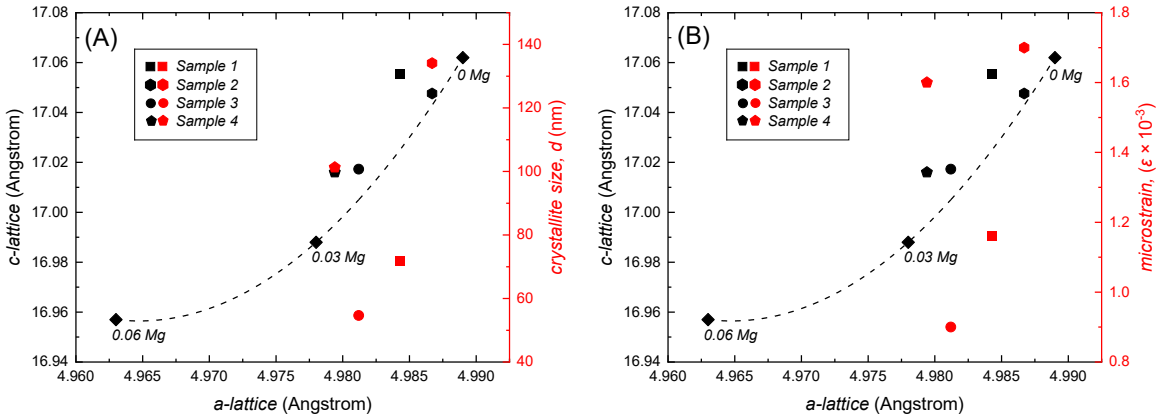

Figure 4. (A) Crystallite sizes; and (B) microstrains with the lattice constants of all the samples. The amount of Mg incorporation in the $CaCO_3$ is indicated by closed diamonds obtained from JCPDS standard patterns for zero- and low-Mg content calcites (Pure calcite: JCPDS 05-0586, $Mg_{0.03}Ca_{0.9}7CO_3$: JCPDS 97-008-6161, and $Mg_{0.06}Ca_{0.94}CO_3$: JCPDS 89-1305).

in the calcites. Hence, the incorporation of Mg atoms could have distorted the calcite lattice, decreasing their crystallite size as lattice distortion creates defects (lattice relaxation) such as dislocations, vacancies, and faults, thereby releasing the stress or microstrain in the calcite [14, 19, 26-27]. TEM analysis of the samples could better measure the actual crystallite size as well as the directly observation of defects in the calcites. This will be a subject for further studies.

Because the limestone samples used for this study were collected close to the marine environment (i.e., cut slopes and boulders by the hill roads along the Sarangani Bay), the calcite was formed in sedimentary environments via biological, chemical and physical processes in the past. Therefore, the limestone samples were most likely formed over time by the deposition and accumulation of dead calcareous material in the form of corals, shells and skeletons of sea animals at the bottom of the sea [38]. Microscopic marine organisms such as planktons and foraminifera extract dissolved calcium and carbonate ions from seawater to build these corals, shells and skeletons. Moreover, the low Mg concentrations in the samples as inferred from the data suggest that the marine environment in which the calcites were formed was during the geologic period when the Mg/Ca ratio in seawater was low [39-40]. Hence, the Mg incorporation into the calcite crystal could have distorted the calcite lattice, forming defects by the release of stress; therefore, reducing the microstrain. Although further studies are needed to validate these observations.

Conclusion

The powder XRD analysis reveals the crystalline characteristics of the natural calcites found from the different locations in Southern Philippines. The distinct Bragg peaks of the samples exhibit well-formed crystalline structures dominated by calcites, and some even featuring an aragonite phase. The calculated lattice constants denote different amounts of Mg incorporation within the calcites. The Williamson–Hall method is modified into the Unified Stress Distribution Method (USDM), to accommodate elastic anisotropy. The Young's modulus value for hexagonal crystals was calculated to be ~100.5 GPa. Comparative study validates both UDM and USDM, revealing consistent crystallite sizes and microstrain values. The anisotropic traits as found in *Sample 2*, was observed most notably by deviations in the crystallite sizes, highlights the pivotal role of USDM. The possible incorporation of Mg atoms could have distorted the calcite lattice and decreased the crystallite size, which in turn results to lattice distortion creating defects (lattice relaxation) such as dislocations, vacancies, and faults. This releases stress and reduces microstrains in the calcites.

The study exhibits the significance of using the USDM of the modified W–H model and enhances understanding of the microstructural complexities of anisotropic calcites, particularly those found in General Santos City and Sarangani Province, Southern Philippines. However, characterizations, such as TEM and X-ray Fluorescence (XRF) are needed to comprehensively understand the calcite limestone in greater detail.

Authors' Contributions

RGB conceptualized the whole research scope and wrote the manuscript, RCB and RJJ carried out the analysis and assisted in the writing, and MI conducted the experiment. All authors have read and agreed to the published version of the manuscript.

Acknowledgments

The authors acknowledge the support of Department of Science and Technology – Philippine Council for Industry, Energy and Emerging Technology Research and Development (DOST–PCIEERD), Advanced Device and Materials Testing Laboratory (ADMATEL), and Materials Science Division – Industrial Technology Development Institute (MSD –ITDI) under the Facilities and Laboratory Access Grant (FLAG). The authors also acknowledge the assistance of Godfrey S. Saloria during the sample preparation.

References

[1] Siegel, F.R. (1967). Chapter 9 properties and uses of the carbonates. *Developments in Sedimentology, 9(B),* 343-393. Doi:10.1016/S0070-4571(08)71036-7

[2] Schwab, F.L. (2003). Sedimentary petrology. (R.A. Meyers, Ed.). *Encyclopedia of Physical Science and Technology (Third Edition),* 459-529. Doi: 10.1016/B0-12-227410-5/00678-5

[3] Gunasekaran, S., Anbalagan, G. and Pandi, S. (2006). Raman and infrared spectra of carbonates of calcite structure. *Journal of Raman Spectroscopy, 37,* 892-899. Doi:10.1002/jrs.1518

[4] Levin, E.M., Roth, R.S. and Martin, J.B. (1961). Polymorphism of ABO_3 type rare earth borates. *The American Mineralogist, 46,* 1030-55.

[5] Sivrikaya, O. (2018). A study on the

physicochemical and thermal characterisation of dolomite and limestone samples for use in ironmaking and steelmaking. *Ironmaking & Steelmaking, 45(8),* 764-772. Doi:10.1080/0301 9233.2017.1337264

[6] Boggs, Sam Jr. (2009). *Petrology of Sedimentary Rocks*. 2nd ed. Cambridge, UK: Cambridge University Press.

[7] Lamar, J.E. (1961). *Uses Of Limestone And Dolomite*. 2nd ed. Urbana, IL: Illinois Geological Survey Library.

[8] Hawkins, P., Tennis, P. and Detwiler, R. (2003). The use of limestone in portland cement: a state-of-the-art review. Skokie, IL: Portland Cement Association.

[9] Sdiri, A., Higashi, T., Hatta, T., Jamoussi, F. and Tase, N. (2010). Mineralogical and spectroscopic characterization, and potential environmental use of limestone from the abiod formation, Tunisia. *Environmental Earth Sciences, 61,* 1275-1287. Doi:10.1007/s12665-010-0450-5

[10] Deng, T.F. and Du, S.C. (2014). Dissolution mechanism of dolomite in converter slag at 1873K. *Ironmaking & Steelmaking, 41(1),* 75-80. Doi:10.1179/1743281212Y.0000000101

[11] Dwarapudi, S., Sekhar, C., Paul, I., Prasad, Y.S., Modi, K. and Chakraborty, U. (2014). Effect of fluxing agents on the swelling behavior of hematite pellets. *International Journal of Mineral Processing, 126,* 76-89. Doi: 10.1016/j.minpr o.2013.11.012

[12] Umadevi, T., Nelson, K., Mahapatra, P.C., Prahbu, M. and Ranjan, M. (2009). Influence of magnesia on iron ore sinter properties and productivity. *Ironmaking & Steelmaking, 36(7),* 515-520. Doi:10.1179/174328109X445741

[13] Oates, J.A.H. (2008). *Lime and Limestone: Chemistry and Technology, Production and Uses*. New York: John Wiley & Sons. 2008.

[14] Banal, R.G. et al. *In preparation*.

[15] Ungár, T. (2006). Microstructure of nanocrystalline materials studied by powder diffraction. *Ninth European Powder Diffraction Conference: Prague, September 2-5, 2004*. *München: Oldenbourg Wissenschaftsverlag,* 313-318. Doi:1 0.1524/9783486992526-053

[16] Maniammal, K., Madhu, G. and Biju, V. (2017). X-ray diffraction line profile analysis of nanostructured nickel oxide: Shape factor and convolution of crystallite size and microstrain contributions. *Physica E: Low-dimensional Systems and Nanostructures, 85,* 214-222. Doi:10.1016/ j.physe.2016.08.035

[17] Madhu, G.M., Bose, V.C., Maniammal, K. Aiswarya Raj, A.S. and Biju, V. (2013). *Physica B: Condensed Matter, 421,* 87-91. Doi:10.1016/ j.physb.2013.04.028

[18] Yogamalar, R., Srinivasan, R., Vinu, A., Ariga, K. and Bose, A.C. (2009). X-ray peak broadening analysis in ZnO nanoparticles. *Solid State Communications, 149 (43-44),* 1919-1923. Doi:10.1016/j.ssc.2009.07.043

[19] Ameh, E. S. (2019). A review of basic crystallography and X-ray diffraction applications. *The International Journal of Advanced Manufacturing Technology, 105,* 3289-3302. Doi:1 0.1007/s00170-019-04508-1

[20] Williamson, G.K. and Hall, W.H. (1953). X-ray line broadening from filed aluminium and Wolfram. *Acta Metallurgica, 1(1),* 22-31. Doi:1 0.1016/0001-6160(53)90006-6

[21] Prabhu, Y.T., Rao, K.V., Kumar, V.S.S. and Kumari, B.S. (2014). X-Ray analysis by Williamson-Hall and Size-Strain plot methods of ZnO nanoparticles with fuel variation. *World Journal of Nano Science and Engineering, 4,* 21-28. Doi:10.4236/wjnse.2014.41004

[22] Rosenberg, Y., Machavariani, V.S., Voronel, A., Garber, S., Rubshtein, A., Frenkel, A.I. and Stern, E.A. (2000). Strain energy density in the X-ray powder diffraction from mixed crystals and alloys. *Journal of Physics: Condensed Matter, 12,* 8081-8088. Doi:10.1088/0953-8984/12/37/307

[23] Mote, V., Purushotham, Y. and Dole, B. (2012). Williamson-Hall analysis in estimation of lattice strain in nanometer-sized ZnO particles. *Journal of Theoretical and Applied Physics, 6(1),* 1 -8. Doi:10.1186/2251-7235-6-6

[24] Venkateswarlu, K., Chandra Bose, A. and Rameshbabu, N. (2010). X-ray peak broadening studies of nanocrystalline hydroxyapatite by Williamson–Hall analysis. *Physica B: Condensed Matter, 405(20),* 4256-4261. Doi: 10.1016/ j.physb.2010.07.020

[25] Sun, J., Wu, Z., Cheng, H., Zhang, J. and Frost, R.L. (2014). A Raman spectroscopic comparison of calcite and dolomite. *Spectrochimica Acta Part A: Molecular and Biomolecular Spectroscopy, 117,* 158-162. Doi: 1

0.1016/j.saa.2013.08.014

[26] Aufort, J. and Demichelis, R. (2020). Magnesium impurities decide the structure of calcium carbonate hemihydrate. *Crystal Growth & Design, 20,* 8028-8038. Doi:10.1021/ acs.cgd.0c01282

[27] Kunitake, M.E., Baker, S.P. and Estroff, L.A. (2012). The effect of magnesium substitution on the hardness of synthetic and biogenic calcite. *MRS Communications, 2 (3),* 113-116. Doi: 10.1557/ mrc.2012.20

[28] Islam, S., Ullah, S.M., Jolly, Y.N., Islam, A. and Biswas, P.K. (2021). Petrological, geochemical, and microfacies analysis of the Sylhet limestone, Bengal basin, Bangladesh: implication for depositional environment and diagenesis. *Arabian Journal of Geosciences*, *14 (1),* 1-22. Doi:10.1007/s12517-020-06308-4

[29] Langford, J.I. and Wilson, A.J.C. (1978). Scherrer after sixty years: a survey and some new results in the determination of crystallite size. *Journal of Applied Crystallography, 11,* 102-113. Doi: 10.1107/S0021889878012844

[30] Cullity, B.D. (1978). *Elements of X-ray Diffraction* (2nd Ed. ed.). Addison-Wesley Publishing Company.

[31] Balzar, D., Audebrand, N., Daymond, M.R., Fitch, A., Hewat, A., Langford, J.I., Le Bail, A., Louër, D., Masson, O., McCowan, C.N., Popa, N.C., Stephens, P.W. and Toby, B.H. (2004). Size–strain line-broadening analysis of the ceria round-robin sample. *Journal of Applied Crystallography*, *37(6),* 911-924. Doi:10.1107/S00 21889804022551

[32] Pandiyarajan, T. and Karthikeyan, B. (2012). Cr doping induced structural, phonon and excitonic properties of ZnO nanoparticles. *Journal of Nanoparticle Research, 14(1),* 647-655. Doi:10.1007/s11051-011-0647-x

[33] Bindu, P. and Thomas, S. (2014). Estimation of lattice strain in ZnO nanoparticles: X-ray peak profile analysis. *Journal of Theoretical and Applied Physics, 8,* 123-134. Doi:10.1007/s40094-014-0141 -9

[34] Zhang, J.-M., Zhang, Y., Xu, K.-W. and Ji, V. (2006). General compliance transformation relation and applications for anisotropic hexagonal metals. *Solid State Communications, 139,* 87-91. Doi:1 0.1016/j.ssc.2006.05.026

[35] Balzar, D. and Ledbetter, H.J. (1993). Voigt function modeling in Fourier analysis of size and strain broadened X-ray diffraction peaks. *Journal of Applied Crystallography, 26,* 97-103. Doi:10.110 7/S0021889892008987

[36] Warren, B.E. and Averbach, B.L. (1950). The effect of cold-work distortion on X-ray patterns. *Journal of Applied Physics, 21,* 595. Doi:10.1063/1.1699713

[37] Peselnick, L. and Robie, R.A. (1962). Elastic constants of calcite. *Journal of Applied Physics, 33,* 2889-2892. Doi:10.1063/1.1702572

[38] Klein, C. and Hurlbut, Jr. C.S., (1993). *Manual Of Mineralogy (after James D. Dana)*. Rev. 21st Ed. New York, NY. John Wiley & Sons, Inc.

[39] Wilkinson, B.H. and Given, R.K. (1986). Secular variation in abiotic marine carbonates: Constraints on phanerozoic atmospheric carbon dioxide contents and oceanic Mg/Ca ratios. *The Journal of Geology, 94(3),* 321-333. Doi:1 0.1086/629032

[40] Hain, M.P., Sigman, D.M., Higgins J.A. and Haug, G.H. (2015). The effects of secular calcium and magnesium concentration changes on the thermodynamics of seawater acid/base chemistry: Implications for eocene and cretaceous ocean carbon chemistry and buffering. *Global Biogeochemical Cycles, 29,* 1-17. Doi: 10.1002/2014GB004986